EFFECT OF SURFACE ROUGHNESS ON ADHESIVE FORCES AND HYSTERETIC ENERGY LOSSES AT THE CONTACT OF TWO NOMINALLY FLAT SURFACES

A Thesis Presented

By

Feng Shen

to

The Department of Mechanical and Industrial Engineering

in partial fulfillment of the requirements
for the degree of

Master of Science

in the field of

Mechanical Engineering

Northeastern University
Boston, Massachusetts

December 2016

ABSTRACT

Hertz Theory (1882) is the classical theory used to solve contact problems of elastic solids without considering the effect of adhesive forces. It was nearly one century later that Johnson, Kendall and Roberts (1971) presented a new theory to study adhesion in the contact of elastic solids. In this thesis, we consider the contact of two elastic planar surfaces, one of which is rough and the other is smooth. Following the procedure of Greenwood and Williamson (1966), the asperity heights are assumed to have a Gaussian distribution with standard deviation σ and all asperities are assumed to have equal radius of curvature at their summits. However, we use the JKR model instead of the Hertz model for each asperity contact. Thus, this procedure is similar to that used by Tabor and Fuller (1975). By applying an approximate form of the JKR load-displacement relation to each single asperity, the total force between the surfaces is obtained during a loading/unloading cycle. However, the behavior during loading and unloading of the rough surface differ. In particular the pull-on and pull-off forces differ because adhesion in the contact produces hysteresis which results in energy loss. The maximum pull-on and pull-off forces in one contact/separation cycle are each a function of the elastic adhesion index which is a measure of the ratio of

surface roughness to adhesion deformation. This key parameter represents the ratio of the dispersion of asperity heights to the maximum extended distance of an asperity above its undeformed position before adhesion is broken. In addition the pull-off force also depends on the maximum extent of loading. It is also shown that for large values of the elastic adhesion index (rough surfaces), not only is the effect of adhesion decreased to a negligible fraction of that for smooth surfaces, but the hysteretic energy losses are significantly decreased.

Keywords: Contact Adhesion, Surface Roughness, Hysteresis, Pull-on/Pull-off, JKR

ACKNOWLEDGEMENTS

I would express my deep sense of gratitude to my advisor ***Prof. George G. Adams*** *for his valuable guidance, timely help and keen encouragement in completing my Master Thesis through the past one and half years. The valuable experience in completing this thesis will be definitely beneficial to the consolidation of the theory knowledge*

I am very grateful to my parents and friends for their incredible love, support and understanding, either financially or physically. Thank you.

LIST OF SYMBOLS AND ABBREVIATIONS

$\boldsymbol{MEMS}$	Micro-Electro Mechanical Systems;
$\boldsymbol{SPM}$	Scanning Probe Microscope;
$\boldsymbol{\gamma, \gamma_1, \gamma_2}$	Surface energy which is the work need per unit area to create a reversibly and isothermally surface;
$\boldsymbol{\gamma_{12}}$	Interfacial energy;
$\boldsymbol{w}$	Dupré energy of adhesion;
$\boldsymbol{U}$	Total potential energy;
$\boldsymbol{\sigma}$	Adhesive stress;
$\boldsymbol{\sigma_0}$	Maximum theoretical stress;
$\boldsymbol{H, h, d}$	Separation between the surfaces;
$\boldsymbol{P, \overline{P}}$	External applied load;
$\boldsymbol{\widehat{P}}$	Total force between the surfaces;
$\boldsymbol{\varepsilon}$	Equilibrium separation;
$\boldsymbol{R_1,\ R_2}$	Radius of the spheres respectively;
$\boldsymbol{R}$	Effective radius of curvature;

$\boldsymbol{a},\ \boldsymbol{a_H}$	Radius of contact area;
$\boldsymbol{a_0}$	Contact radius under zero applied load upon loading;
$\boldsymbol{a_c}$	Contact radius when pull-off occurs;
$\boldsymbol{F_0}$	Pull-off forces upon unloading for different contact models;
$\boldsymbol{K}$	Elastic constant;
$\boldsymbol{\nu}$	Poisson's Ratio;
$\boldsymbol{E^*}$	Effective Young's Modulus;
$\boldsymbol{\delta, \Delta}$	Approach (Interference);
$\boldsymbol{z}$	Asperity height;
$\boldsymbol{\mu}$	Tabor parameter;
$\boldsymbol{\delta, \delta_H}$	Approach (Interference);
$\boldsymbol{\delta_c, \Delta_c}$	Maximum extended distance above its undeformed and original height of a single asperity and amount of asperities;
$\boldsymbol{\delta_0}$	Approach under zero applied load upon loading;
$\boldsymbol{M-D}$	Maugis-Dugdale (M-D) model;
$\boldsymbol{JKR}$	Johnson- Kendall- Roberts Model;
$\boldsymbol{DMT}$	Derjaguin-Muller-Toporov Model;

$\boldsymbol{\lambda}$	Maugis elastic parameter;
$\boldsymbol{\phi(z)}$	Gaussian distribution of asperity heights;
$\boldsymbol{\sigma}$	Standard deviation;
$\boldsymbol{N, n}$	Number of asperities;
$\boldsymbol{p(r)}$	Pressure distribution;
$\boldsymbol{p_0}$	Maximum contact stress;
$\boldsymbol{P_1}$	Effective Hertz load;
$\boldsymbol{\psi}$	Non-dimensional parameter: relation between $\frac{P}{P_c}$ and $\frac{\delta}{\delta_c}$;
$\boldsymbol{P_{loading}}$	Total force per unit area during loading;
$\boldsymbol{P_{unloading}}$	Total force per unit area during unloading;
$\boldsymbol{\overline{P_1}}$	Total force during unloading by the distance to a maximum separation of Δ_c;
$\boldsymbol{\overline{P_2}}$	Transition total force during unloading by the distance to a separation of $h - h_0$;
$\boldsymbol{L}$	Lower limit of the integration which to determine P_{off};
$\boldsymbol{h_0}$	Minimum separation due to how much load applied during loading;

$\boldsymbol{P_m, P_m'}$	Maximum pull-off and pull-on forces which will reach in an actual loading/ unloading cycle;
$\boldsymbol{h_m}$	Separation at where maximum pull-off force occurs;
$\boldsymbol{h_{m'}}$	Separation at where maximum pull-on force occurs;
$\boldsymbol{\overline{h_0}}$	Separation at where zero total force between surfaces is upon loading;
$\boldsymbol{\overline{P_m}}$	Pull-off force during unloading from the separation $\overline{h_0}$;
$\boldsymbol{\overline{h_m}}$	Separation at where maximum $\overline{P_m}$ occurs;
$\boldsymbol{\alpha}$	Elastic adhesion index.

TABLE OF CONTENTS

1. INTRODUCTION

1.1 Overview

If the elastic solid surfaces are brought sufficiently close together, there will exist attractive atomic forces between them. As the separation between the two elastic surfaces is decreased, the atomic forces will increase until the surfaces are brought into final contact. Tabor et al. [1] and Israelachvili et al. [2] presented a measure of van der Waals forces to study how the atomic forces varied with the separation between the surfaces. In order to separate the contacting bodies, a force which described as the force of adhesion is needed. Adhesion plays an effective role in nanoscale contacts, especially in micro-electro mechanical systems (MEMS) and in some other related fields, such as nanotribology, nanomanipulation, nanowear and scanning probe microscope (SPM) measurements. As one of the major factors, the effect of adhesion limits the widespread use of micro-electro mechanical systems (MEMS) because of a very large surface to volume ratio. Zhao et al. [3], Maboudian [4] and Feynman [5] are invaluable resources that presented adhesion effects producing public attention in the MEMS field.

For a long time, a well-known theory known as Hertz contact of studying the contact area between elastic solid bodies was given by Hertz [6]. However, the Hertz theory did not consider the adhesion. Hertz theory is appropriate for the contact problems of sufficiently weak surface energy and relatively large applied force. However, surface

energy γ cannot be ignored for nano-contact problems. Energy is required for creating a new solid surface due to bonds broken and atoms reorganization near the surface. Surface energy γ is the work that needed to create a unit surface area reversibly and isothermally. When a solid surface contacts with another one, the Dupré energy of adhesion w, also as known as the work of adhesion, is required to separate two solid surfaces in the reversible and isothermal case. Thereby, the work per unit area to separate two solid surfaces is described as the work of adhesion which is given by $w = \gamma_1 + \gamma_2 - \gamma_{12}$. γ_1 and γ_2 are the surfaces energies of two solid bodies respectively, whereas γ_{12} is the interfacial energy. For the contact of identical bodies, the work of adhesion $w = 2\gamma$ due to the lack of interfacial energy acting between the two bodies. The potential energy (U) is a function of the separation (H) between two solid surfaces which is given by the Lennard-Jones potential. This potential energy (U) quantity, is defined as $U(H) = -\frac{4w}{3}\left[\left(\frac{\varepsilon}{H}\right)^2 - \frac{1}{4}\left(\frac{\varepsilon}{H}\right)^8\right]$, where ε is the equilibrium separation between two surfaces is well defined by Yu and Polycarpou [7]. The potential energy will reach minimum if the separation of surfaces is equal to the equilibrium separation (ε) specifically. Furthermore, the adhesive stress (σ) is also a function of the separation of the surfaces by deriving the potential energy (U) with respect to the separation (H), is given by $\sigma(H) = -\frac{8w}{3\varepsilon}\left[\left(\frac{\varepsilon}{H}\right)^3 - \left(\frac{\varepsilon}{H}\right)^9\right]$. The adhesive stress ($\sigma$) will reach the maximum value, also known as theoretical stress (σ_0), which is given by $\sigma_0 = \frac{16w}{9\sqrt{3}\varepsilon}$.

1.2 Rigid Contact Model

1.2.1 Bradley Model

A van der Waals model, also well known as Bradley model [8] provided a method of calculating the tensile force between two perfectly rigid and smooth spheres which was given. Bradley model was based on the contact between two rigid spheres with radius R_1 and R_2 respectively. The adhesive force between two bodies was determined by integrating the van der Waals forces. When two contacting bodies were separated, the relative pull-off force upon unloading was found to be $F_0 = -2\pi Rw$, where R was the effective radius of curvature (i.e. $\frac{1}{R} = \frac{1}{R_1} + \frac{1}{R_2}$).

The negative sign represented the tension between two rigid spheres with smooth surfaces. Bradley model considered the intermolecular forces as the surface forces. The separation between two rigid surfaces of Bradley model was defined as $\mathrm{H} = r^2/2R$. Therefore, the adhesive interaction was given by $F = -\int_0^\infty 2\pi r\sigma(H)dr = -2\pi R\int_0^\infty \sigma(H)dH = -2\pi Rw$.

1.3 Elastic Adhesion Contact Model

1.3.1 Johnson, Kendall and Roberts (JKR) Model

As Hertz theory was compared with experiments between rubber and glass spheres contact, several theories and contradictions were presented in the late 1960s.

Johnson, Kendall and Roberts [9] revised and complemented the classical Hertz theory, then presented a new theory to study adhesion in the contact of elastic solids. The Johnson-Kendall-Roberts (JKR) theory was the first to incorporate the effect of adhesion into Hertz contact. Observed by the JKR model, Hertz theory was suitable for integrating contact area at large loads. However, the contact area at low loads predicted by JKR model was larger than that predicted by Hertz theory due to the elastic deformation caused by the tensile (attractive) intermolecular surface forces. The JKR model accounted for adhesive forces within the contact region and neglected the adhesion effect outside the contact area. Furthermore, if the externally applied load was removed, the contact area would still have a non-zero value. Meanwhile, the adhesive force between the contacting surfaces was very strong in case of the surfaces were dry and clean.

The JKR model did consider the adhesion effect appropriately which also included the Dupré energy of adhesion (w). The pull-off force to separate the contacting surfaces was determined by minimizing the potential energy (U) which was given by $F_0 = -\frac{3}{2}\pi R w$. Thus, it can be seen the pull-off force was less than that predicted by Bradley model for rigid contact (i.e. $-2\pi R w$). Assume that if the Dupré energy of adhesion (w) vanishes, the JKR theory will be reduced to Hertz contact. It is necessary to note that the conclusion obtained from JKR model only includes elastic deformation. We use JKR

model throughout this thesis for considering the contact of two elastic planar surfaces. The detailed statements on JKR model will be carried out in the following chapter.

1.3.2 Derjaguin-Muller-Toporov (DMT) Model

The tensile force between two perfectly rigid spheres was given by Bradley model. Derjaguin-Muller-Toporov [10], [11] incorporated Hertz model and Bradley model, and presented a modified model for the contact of two elastic spheres with high stiffness. DMT model assumed that there only existed attractive forces outside of the contact area, unlike the JKR model. However, the same contact profile and model geometry are still same as in the Hertz contact are assumed by the DMT model, but with an increased attractive traction. Thus, the contact radius was larger than that predicted by Hertz theory due to the additional attraction outside the contact region which is given by $a^3 = \frac{R(P+2\pi Rw)}{K}$, where a is contact radius and K is the elastic constant defined by $K = \frac{4E^*}{3}$. Meanwhile, the approach (δ) is given by $\delta = a^2/R$. From the equations, it is clear that the contact radius $a_0^3 = \frac{2\pi wR^2}{K}$ when there is no external load applied upon loading. During the subsequent unloading, the separation between the surfaces is produced at zero contact radius. Although there is adhesive attraction between surfaces before coming into contact, no deformation is likely to occur. Therefore, the shape of spheres does not change. The pull-off force during unloading cycle is therefore obtained as same as the adhesion force predicted by Bradley model. The same behavior of loading and unloading produces no hysteresis losses due to

the same values of pull-on and pull-off force. Unlike the JKR model, when the contact area is reduced to zero at separation the pull-off force is acquired and the behavior of both spheres become rigid.

1.3.2 Tabor Parameter (μ)

From the JKR and DMT models, it is obvious that different pull-off forces are achieved by the two models. This apparent contradiction is well resolved after the Tabor parameter (μ) [12] is introduced. Tabor [12] indicated that the JKR model is applicable to cases of a small ratio of the range of surfaces force to the elastic deformation while the DMT model suits the larger ratio. The appearance of a necked region was observed closely outside the contact edge of two spheres by light microscope (LM). The neck height (h_c) is equal to $\left(\frac{Rw^2}{E^{*2}}\right)^{1/3}$ which was given by Tabor [12]. According to the height of neck h_c over the equilibrium separation (ε), a dimensionless Tabor parameter (μ) was given by $\mu = \left(\frac{Rw^2}{E^{*2}\varepsilon^3}\right)^{1/3}$. Tabor parameter ($\mu$) is a measure of the ratio of the elastic deformation to the effective range of surface forces. Tabor pointed that JKR model is in good agreement with the experimental results as Tabor parameter (μ) is approximately greater than 3, whereas DMT model is much closer to the reality as Tabor parameter (μ) is approximately less than 0.1.

1.3.3 Maugis Model

Maugis [13] presented an analytical model using the model of Dugdale crack [14], as well-known as the Maugis model which accounts for a continuous transition between the JKR and DMT theories. Thus, the Maugis model is occasionally referred as the Maugis-Dugdale (M-D) model. The Maugis model is the most accurate theory in past decades which is applicable to any contact mechanics problems of spheres with either strong or weak adhesion. For the Maugis model, the adhesive molecular force is assumed acting within a ring region near the edge of the contact area border. With using the Dugdale model [14] of elastic-plastic fracture mechanics, the Maugis model assumes that the adhesive stress is equal to the theoretical stress (σ_0) when the local separation between surfaces is less than a critical value of h_0, whereas the adhesive stress is reduced to zero when the local separation is greater than h_0. Therefore, the work of adhesion is given by $\mathrm{w} = \sigma_0 h_0$, where the theoretical stress (σ_0) is given by $\sigma_0 = \frac{16w}{9\sqrt{3}\varepsilon}$ as talked above based on the Lennard- Jones potential. Thus, the prescribed value of separation h_0 is obtained, $h_0 = \frac{w}{\sigma_0} \cong 0.97\varepsilon$. The adhesion of Maugis model (also known as the M-D model) [3] is determined by a non-dimensional elastic parameter (λ) which is related to the Tabor parameter (μ). The Maugis elastic parameter (λ) is described as $\lambda = 2\sigma_0 \left(\frac{R}{\pi w K^2}\right)^{1/3} \cong 1.16\mu$. The JKR and DMT models are particular cases of the Maugis model which are determined by different values of the Maugis parameter (λ). The JKR model (compliant

materials) is applicable for $\lambda \to \infty$, whereas as $\lambda \to 0$ the DMT model (stiff materials) is valid. Therefore, Maugis model describes a transition model between the JKR (valid for λ is greater than about 3) and DMT (valid for λ is less than about 0.1) models.

1.4 Statement of the Problem

As one of the major factors, the effect of adhesion limits the widespread use of micro-electro mechanical systems (MEMS) and nanotechnology due to scaling effects. Let's consider about the dimensions change of the JKR model to prove the importance of adhesion. The adhesive pull-off force of the JKR model is expressed as $F_0 = -\frac{3}{2}\pi R w$, where the unit of the Dupré energy of adhesion (w) is $\mathrm{J/m^2}$. Meantime, the maximum value of the adhesive stress is expressed as $\sigma_0 = \frac{16w}{9\sqrt{3}\varepsilon}$. It is clear that as dimensions change from millimeters (mm) to nanometers (nm), the weight of contacting bodies decreases by a factor of 10^{18} and the relative adhesive pull-off force decreases by a factor of 10^6. However, the importance of adhesion stress increases by a significant factor of 10^{12}. Similarly, the same scaling effects apply to the DMT and Maugis models. Thus, it can be proven that the adhesion effect cannot be ignored in MEMS and nanotechnology fields.

In fact, the surface roughness is in micro- or nano-scale with respect to the nominal contact region of surfaces. Johnson, Kendall and Roberts [9] complemented the classical Hertz theory which is the original elastic contact theory, and then presented the well-known JKR theory to study the elastic adhesion. Greenwood et al. [15] analyzed the adhesionless

contact of two nominally rough surfaces with using Exponential distribution and Gaussian distribution of asperity heights of the surfaces respectively. Fuller and Tabor [16] investigated the effect of surface roughness on the reduction of the elastic adhesion.

The aforementioned JKR model described the adhesion between theoretically smooth elastic surfaces. For this reason, we will revise the contact model in consideration of randomly distributed surface roughness while using the JKR model for individual asperities in the thesis. Using Maugis theory, Johnson and Greenwood [17] provided an adhesion map for the contact of elastic spheres which is very useful.

Adhesion hysteresis is described as the difference between the work done to separate two surfaces during unloading and that initially acquired on bringing them together into contact upon loading. Both the JKR and Maugis models accounted for the existence of hysteresis due to the different behaviors during a contact/separation cycle. Hysteretic energy losses are a very common phenomenon which cannot be ignored in small-scale interface and surface interactions. However, for some contacting systems with small scale dimensions, hysteresis losses are most obvious. Especially, hysteresis losses will be embodied in a phase shift between the driving excitation and the oscillation of the tip when the tapping mode is manipulated by the atomic force microscope (AFM) [18], [19], [20], [21]. As the Tabor parameter (μ) increases, Muller et al. [22] presented a complete calculating method to show how the behavior changed from the DMT model to the JKR

model. They showed that when the Tabor parameter (μ) is greater than five, the maximum pull-off force is achieved very nearly the same as the JKR theory. Ciavarella et al. [23] pointed out that when the Tabor parameter (μ) is greater than five, the hysteresis loss is very close to the numerical solutions based on the JKR load-displacement curve with using the Lennard- Jones potential.

In the thesis, we focus on the contact of two elastic planar surfaces, one of which is rough and the other is smooth. Following the procedure of Greenwood and Williamson [15], the asperity heights of surfaces are assumed to have a Gaussian distribution. We develop an approximate solution based on the JKR load-displacement relation and apply to each single asperity which as same as the Fuller and Tabor analysis. Thus, the different loading and unloading paths for different surface roughness are obtained. The total force between the surfaces is further obtained during a loading/unloading cycle. We revise the Fuller-Tabor model and obtain the adhesive forces (the pull-on and pull-off forces) for variable surface roughness. It is shown that the hysteresis loss and the adhesive forces are affected by a non-dimensional parameter (adhesion index, which is a measure of the ratio of surface roughness to adhesion deformation) and by the non-dimensional extent of loading.

2. PROBLEM FORMULATION

Following the procedure of Greenwood [24], the experimental results show that the *Gaussian distribution* is a very good approximation for asperity heights of many surfaces. Therefore, we use a *Gaussian distribution* of asperity heights to treat the surface roughness, i.e.

$$\phi(z) = \frac{1}{(2\pi)^{\frac{1}{2}}} \exp\left(-\frac{z^2}{2\sigma^2}\right) \tag{1}$$

where σ is the standard deviation and $\phi(z)\,dz$ represents the probability of an asperity having a height between z and $z + dz$ above the mean, with the corresponding mean of asperity heights at $z = 0$.

Note that for sake of simplicity, we could assume the peak of each asperity as a sphere with the radius R when the rough surface contacting with a perfectly flat surface. Mean surface height is average level of the surface, whereas mean summit height, a crucial concept throughout this thesis, is the mean level of all the peaks of asperities. The separation d is the distance between the mean of asperity heights and the perfectly flat surface. If the height of those peaks exceeds the separation d, the asperities and flat smooth surface are compressed each other by a distance δ as shown in Figure 1. Assuming that there are totally N asperities per unit area, a series of peaks n which will make contact with that flat plane is given by [15],

$$n = N \int_d^\infty \phi(z)\,dz \tag{2}$$

Firstly, Hertz [6] advanced a theory which considering the contact between two elastic smooth spheres. The two spheres are perfectly elastic with radius R_1 and R_2 respectively, thus the Hertz contact only investigated the elastic deformation of the spheres. The spheres are brought together and pressed each other under an applied load $\bar{P}$. Therefore, a circular contact region was made which the contact radius a_H is given by

$$a_H = \left(\frac{\bar{P}R}{K}\right)^{1/3} \tag{3}$$

where K is the elastic constant defined as

$$K = \frac{4E^*}{3} \tag{4}$$

where E^* is the effective Young's modulus and R is the effective radius of curvature defined as

$$\frac{1}{E^*} = \frac{1-\nu_1^2}{E_1} + \frac{1-\nu_2^2}{E_2} \tag{5}$$

$$\frac{1}{R} = \frac{1}{R_1} + \frac{1}{R_2} \tag{6}$$

where E_1 and E_2 are the elastic Young's moduli of contact bodies respectively, and ν_1 and ν_2 are the Poisson's ratios of two bodies respectively. The displacement δ_H of distant points in spheres is introduced due to the compression which given by,

$$\delta_H = \left(\frac{\bar{P}}{KR^{1/2}}\right)^{2/3} \tag{7}$$

In the meantime, the pressure distribution is described as

$$\mathrm{p(r)} = p_0 \left(1 - \frac{r^2}{{a_H}^2}\right)^{\frac{1}{2}} \tag{8}$$

where the maximum contact stress $p_0 = 3\bar{P}/2\pi {a_H}^2$.

It had been several decades that Hertz Theory [6] without considering the effect of adhesive forces was fully accepted and fashionable until the JKR theory was developed. When a nominally rough surface makes contact with a flat smooth surface, the local pressure is obviously high at the contact region because of the random height of asperities, resulting in the real contact area. In order to incorporate and improve the Hertz theory, a new theory was formulated by Johnson, Kendall and Roberts [9] in the presence of adhesion. JKR theory studied the effect of adhesion at the contact region as well as contact pressure with using a balance between the loss in surface energy and the stored elastic energy. Compared with Hertz Theory, an increase of contact area is produced by JKR model as Figure 2 shows. Following the JKR model, we apply an external *Load P* to compress a spherical asperity with the radius of the curvature R. The pressure distribution of the JKR model is given by Johnson, Kendall and Roberts [9],

$$\mathrm{p(r)} = p_0 \left(1 - \frac{r^2}{a^2}\right)^{\frac{1}{2}} + p_0' \left(1 - \frac{r^2}{a^2}\right)^{-\frac{1}{2}} \tag{9}$$

$$p_0 = \frac{2aE^*}{\pi R}\ ,\ p_0' = -2\left(\frac{\gamma E^*}{\pi a}\right)^{-\frac{1}{2}} \tag{10}$$

where γ is the surface energy of each surface per unit area. Also note that the pressure distribution of the JKR model, a new term is included which contains p_0' due to the tensile force sustained in the contact region as shown in Figure 2. As usual we define the work done per unit area in separating two bodies as w, namely the work of adhesion. The contact radius a of contact area in the JKR model can be written in the presence of surface energy, which are modified by Johnson, Kendall and Roberts [9],

$$a^3 = \frac{P_1 R}{K} \tag{11}$$

$$P_1 = P + 3\pi wR + \sqrt{6\pi wRP + (3\pi wR)^2} \tag{12}$$

$$a = \left(\frac{\left(P + 3\pi wR + \sqrt{6\pi wRP + (3\pi wR)^2}\right)R}{K} \right)^{1/3} \tag{13}$$

where P_1 is the effective Hertz load due to adhesion acting between the elastic contact bodies. The approach δ of distant points in two surfaces which represents the displacement between the peak of the single asperity and the flat smooth surface is given by Tabor and Fuller [16],

$$\delta = \frac{Ka^3 + 2PR}{3RKa} \tag{14}$$

In [16], the experiments were carried out on the contact of rubber spheres and flat Perspex surface which are both smooth.

From Eqn. (12), it is obvious that the effective Hertz load P_1 is greater than applied load P due to the surface energy effect. Meanwhile in absence of the work of adhesion, the contact radius reduces to simple Hertz Contact equation, i.e.

$$a = \left(\frac{PR}{K}\right)^{1/3} = \left(\frac{3PR}{4E^*}\right)^{1/3} \tag{15}$$

Note that the contact area between two elastic bodies maintains zero until loading from zero applied load. Therefore, no deformation occurs until contact on the basis of JKR theory. At the initial moments of loading, the applied load still is zero while the contact area is finite due to the sudden effect of adhesive forces. Under the effect of zero external loads (i.e. P=0), the contact becomes finite and is given by using Eqn. (13),

$$a_0 = \left(\frac{6\pi w R^2}{K}\right)^{1/3} \tag{16}$$

Using Eqn. (14), the approach under zero applied load is, therefore:

$$\delta_0 = \frac{a_0^2}{3R} = \left(\frac{4\pi^2 w^2 R}{3K^2}\right)^{1/3} \tag{17}$$

Due to the work energy of adhesion, two elastic bodies will still be in contact even if the compressively applied load P reduces from positive to zero (i.e. unloading). Now it is necessary to make the applied force negative (tensile force) to separate the asperity and the smooth elastic surface. The separation occurs when the *tensile force* reaches a maximum critical value is given by [9], [25], as

$$P_c = \frac{3}{2}\pi w R \tag{18}$$

where P_c represents the pull-off force (tensile) for breaking the adhesion between the single asperity and the flat smooth surface. Then separation occurs.

The corresponding contact radius and approach are given by Eqns. (13) and (14), i.e.

$$a_c = \left(\frac{3\pi w R^2}{2K}\right)^{1/3} \tag{19}$$

$$\delta_c = \frac{a_c^2}{3R} = \left(\frac{\pi^2 w^2 R}{12K^2}\right)^{1/3} \tag{20}$$

By combining Eqns. (13), (14), (19) and (20), we can simply express these equations non-dimensionally by introducing a parameter ψ, i.e.

$$\frac{\delta}{\delta_c} = (3\psi - 1)\left\{\frac{1}{9}(\psi + 1)\right\}^{\frac{1}{3}} \tag{21}$$

where the non-dimensional parameter ψ can be written in terms of the expression $\frac{P}{P_c}$

$$\psi = \left(\frac{P}{P_c} + 1\right)^2 \tag{22}$$

Inverting this relation between Eqns. (21) and (22), $\frac{P}{P_c}$ can be obtained as a function of $\frac{\delta}{\delta_c}$

$$\frac{P}{P_c} = F\left(\frac{\delta}{\delta_c}\right) \tag{23}$$

where P_c is the maximum tensile force required to make separation occur upon unloading, and δ_c is the maximum extended distance above its undeformed and original height of a single asperity. In this paper, we obtained a *Four-term Curve-fit Piecewise Function* of the

above Eqn. (23) using MATLAB. The *original function* (i.e. Eqns. (21) and (22)) and the *Four-term Curve-fit Piecewise Function* are both plotted as shown in Figure 2.

By using Eqns. (1), (2), and (23), there are *n* asperities will make contact with the smooth surface of N asperities per unit area. Therefore, the total contact force per unit area when two surfaces are making surfaces contact with each other is equal to the summation of the forces applied to the asperities whose height exceeds the separation d above the mean,

$$\hat{P} = nP(z) = N\int_d^\infty P(z)\,\phi(z)dz = \frac{NP_c}{\sigma(2\pi)^{\frac{1}{2}}}\int_d^\infty F\left(\frac{\delta}{\delta_c}\right)\exp\left(-\frac{z^2}{2\sigma^2}\right)dz \tag{24}$$

In order to study the adhesion effect between the flat surface and all of the peaks whose height is greater than d, the parameters of displacement in Eqn. (24) should be expressed in terms of σ which is the standard deviation of asperities heights, i.e.

$$\Delta = \delta/\sigma\,,\ \ \Delta_c = \delta_c/\sigma\,,\ \ h = d/\sigma \tag{25}$$

where d is the separation between the flat smooth surface and the mean level of asperities heights, as talked above. If we assume the height of asperity is z, then the separation δ can be expressed as,

$$\delta = z - d \tag{26}$$

Substituting Eqns. (25) and (26) into (24), therefore the Eqn. (24) becomes,

$$P_{loading} = \frac{NP_c}{(2\pi)^{\frac{1}{2}}}\int_0^\infty F\left(\frac{\Delta}{\Delta_c}\right)\exp\left(-\frac{1}{2}(\Delta + h)^2\right)d\Delta \tag{27}$$

where $P_{loading}$ is the dimensionless total force per unit area upon loading. It is obviously noted that $P_{loading}$ is a function of $\mathrm{h} = \mathrm{d}/\sigma$ with a single parameter $\alpha = 1/\Delta_c = \sigma/\delta_c$. When the two surfaces are brought together, the total force between surfaces is compressive which determined by Eqn. (27). We assume that two surfaces are compressed to a minimum separation d_0, which means the minimum separation d_0 depends on how much load applied upon loading (i.e. determined by Eqn. (27)). After that, in order to determine the pull-off force between surfaces upon unloading, the separation d is then increased. The separation will be increased up to the maximum extended distance δ_c above its undeformed and original height of asperities as the adhesion is finally broken between adhering asperities and perfect smooth surface. At this moment, the total force is tensile due to adhesion. Therefore, the total force upon unloading to be determined is different from the loading force in Eqn. (27). Note that the total pull-off force will be found if the lower limit of integration in Eqn. (27) is altered, i.e.

$$\overline{P_1} = \frac{NP_c}{(2\pi)^{\frac{1}{2}}} \int_{-\Delta_c}^{\infty} F\left(\frac{\Delta}{\Delta_c}\right) \exp\left(-\frac{1}{2}(\Delta + h)^2\right) d\Delta \tag{28}$$

where $\overline{P_1}$ represents the total force upon unloading by the distance to a maximum separation of Δ_c. However, as talked above, the total force upon unloading depends on how much load applied during loading (i.e. pull-on force) which varies as the dimensionless minimum separation h_0 change.

Therefore, the transition total force upon unloading is given by

$$\overline{P_2} = \frac{NP_c}{(2\pi)^{\frac{1}{2}}} \int_{-(h-h_0)}^{\infty} F\left(\frac{\Delta}{\Delta_c}\right) \exp\left(-\frac{1}{2}(\Delta + h)^2\right) d\Delta \tag{29}$$

By combining Eqns. (28) and (29), the actual total force upon unloading is given by

$$P_{unloading} = \frac{NP_c}{(2\pi)^{\frac{1}{2}}} \int_{-L}^{\infty} F\left(\frac{\Delta}{\Delta_c}\right) \exp\left(-\frac{1}{2}(\Delta + h)^2\right) d\Delta \tag{30}$$

where the lower limit of the integration is equal to the smaller value of the lower limits in Eqns. (28) and (29), which are given by

$$\mathrm{L} = \begin{cases} (h - h_0) & (h - h_0) < \Delta_c \\ \Delta_c & \Delta_c < (h - h_0) \end{cases} \tag{31}$$

respectively. Therefore, the pull-off force which is maximum tensile force upon unloading follows the dimensionless parameters Δ_c and h_0. It is varied as both Δ_c and h_0 change which is indicated by Eqns. (30) and (31).

3. RESULTS AND DISCUSSION

3.1 Numerical Force-Displacement Relation

Figure 3 shows the force-displacement relation for a single asperity in the presence of the adhesion. P_c is the maximum tensile force required to make separation occur upon unloading, whereas δ_c is the maximum extended distance above its undeformed and original height of a single asperity due to adhesion. Both P/P_c and δ/δ_c are non-dimensional here as shown in Figure 3. P_c is the tensile force at the point 3, whereas δ_c is the separation of the point 4. For a single asperity, the force between the contacting bodies increases sharply at the initial moment of touching as shown from point 1 to 2. The path 1-2 represents the procedure of loading. For the JKR model, the adhesion exists in the contact region when the asperity makes contact with the undeformed plane. At sufficiently small separation, the single asperity and the flat smooth surface will repel each other. The force between the contacting bodies is the equilibrium of repulsive and adhesive forces at the contact region. At the point 2, the system is under zero force and reach the equilibrium state which means the repulsive force is equal to the adhesive force. As more external load is applied on the single asperity, the separation δ will increase continuously and is determined by the extent of loading. The path 2-1-3-4-5 (i.e. from 2 to 5) represents breaking down the adhesion between the single asperity and the undeformed plane, and therefore separating the contact under prescribed force. The tip of single asperity is regarded as a sphere as discussed before. Note that if the subsequent unloading occurs at

the point 2, the contact is remained even though the force reduces to zero in the presence of adhesion. Then it is necessary that the force P should reduce to negative (tension) to break the adhesion. At the point 3, the force P reaches maximum tensile value required to separate the contact which the value is equal to P_c. At the point 4, the single asperity reaches the maximum extension δ_c above its original height. Following that by the path 4-5, the jump-out occurs. For a single asperity, the adhesion between the contacting bodies will be broken once the applied force P reaches the critical tensile value. P_c is therefore the pull-off force which is required to separate the contact. However, the pull-on force is the force at point 1.

When the tip of the single asperity and the undeformed plane coincide at $\delta = 0$, P/P_c is required to be computed for further discussion of pull-on force in this thesis. Substituting $\delta = 0$ into Eqn. (14), the relation between P and P_1 is obtained (i.e. $P_1 = -2P$). In the circumstance of this relation, $P = \frac{4}{3}\pi wR$ is given by Eqn. (12). Therefore, we can get $P/P_c \approx 0.889$ in term of Eqn. (18) for $\delta/\delta_c = 0$. According to the curve-fit function we use throughout the thesis, $P/P_c = 0.883$ for $\delta/\delta_c = 0.01$. The curve-fit function is proved to be effective when comparing the result to the theoretical one with the error is approximately equal to 0.67%.

3.2 Loading/Unloading Paths

In Figures 4 through 9, the normalized force upon loading and unloading is plotted against separation for $\alpha = 1/\Delta_c$= 0.25, 0.5, 1.0, 1.5, 2.0 and 2.5 respectively. When the two surfaces are brought in close, loading is from zero applied load and up to relative load in terms of the minimum separation between the surfaces. Bearing in mind the previous points, subsequent unloading follows by the continued loading. That is to say, the pull-off force depends on how much load is applied upon loading which is based on the minimum separation h_0. In this situation, it is clear that the subsequent pull-off force is also varying at different values of Δ_c and h_0 as explained by Eqns. (30) and (31).

To illustrate how the pull-on and pull-off forces vary, we take Figure 4 as an example. In figure 4, P_m and $P_m{}'$ represent the maximum pull-off and pull-on force respectively, whereas h_m and h'_m are the corresponding separations where P_m and $P_m{}'$ occurs. According to Eqns. (27) and (30), loading and unloading curves are functions of separation h with a parameter $\alpha = 1/\Delta_c = 0.25$. In the meantime, transition curves are plotted at different values of minimum separation $h_0 = -1.5,\ -1,\ -0.5,\ 0,\ 0.5,\ 1$ and 1.5 respectively in terms of Eqn. (31). For $h_0 = 0$, it presents the mean level of asperities heights and the rigid flat surface appear to overlap before unloading. Initially, loading occurs from zero applied load following the path A shown in Figure 4, then unloading occurs as the mean level overlaps the rigid smooth plane which following the path B and

subsequent path C. However, the pull-off and pull-on force do not reach the maximum values P_m and $P_m{}'$ in this case for $h_0 = 0$. Similarly, loading and unloading are varying at different values of h_0 for $\alpha = 1/\Delta_c = 0.25$. When the deformable rough surface and the flat smooth surface approach each other at a sufficient level which means the minimum separation h_0 is small enough, the pull-on and pull-off force will reach the maximum values shown in the Figure 4. Similar results for higher values of parameter $\alpha = 1/\Delta_c$ are described and plotted in Figures 5-9. In general, what these indicates how much load applied upon loading decide the relative pull-off force upon unloading.

Note that results have been obtained for normalized force upon loading and unloading as a function of the separation h, for different values of two pivotal parameters $\alpha = 1/\Delta_c$ and h_0 defined in the JKR model. As discussed above, the normalized separation is larger than $(\Delta_c + h_0)$ during the unloading (Path C) in Figure 4, the lower limit of the integration in Eqn. (30) is $-\Delta_c$ which is independent of the minimum separation h_0, namely, independent of the loading. However, during the transition (Path B), the normalized separation is less than $(\Delta_c + h_0)$, the lower limit of the integration in Eqn. (30) is $-(h - h_0)$. As far as concerned, it is necessary to emphasize that only elastic deformation is included in JKR model, rather than plastic deformation. Therefore, the difference between the loading and unloading behavior which produces hysteresis losses in the presence of adhesive forces of the elastic contact problem. In Figures 4-9, for the given Δ_c and h_0,

the hysteretic energy is equal to the corresponding figure area enclosed by loading, transition and unloading curves under coordinate system. For instance, the hysteretic energy for $\Delta_c = 0.25$ and $h_0 = 0$ in Figure 4 is the area enclosed by Path A, B and C.

3.3 Hysteresis Losses

Figure 10 shows the non-dimensional hysteretic energy losses for a range of values of the minimum separation h_0 for different $\alpha = 1/\Delta_c$. Hysteresis losses are determined by numerical integration of the corresponding areas in Figures 4-9 and depend on the loading and unloading cycles. To determine the hysteresis losses in a contact/separation cycle, Δ_c and h_0 are required. For a given $\alpha = 1/\Delta_c$, the more strenuously loaded the contact, the greater is the hysteresis losses for this multi-asperity JKR model. h_0 is determined by the applied force as given by the force-displacement relations described by Eqn. (28). With regard to the maximum hysteretic energy, it is theoretically equal to the area enclosed by the loading and the unloading curves as shown in Figures 4-9. Thus, as more load is applied to the contact, the possible hysteresis losses will increase from zero to the maximum value as the corresponding dashed lines shown in Figure. 10.

Turning now to the question of what is the relation between the hysteretic energy and the key parameter $\alpha = 1/\Delta_c$ for a given minimum separation h_0? Having considered the parameter $\alpha = 1/\Delta_c = \sigma/\delta_c$, the quantity is the more directly measure of surface roughness which can be defined as elastic adhesion index [26]. For a high roughness

surface, the values of $\alpha = \sigma/\delta_c$ is relatively large because of the large values of σ. The compressive total forces which are exerted by those higher asperities will offset the adhesive (tensile) forces obtained by the lower heights of asperities at any separation. Figure 10 also shows the smoother the surface is, the larger hysteresis losses is sustained for any given minimum separation h_0.

3.4 Maximum Pull-On and Pull-off Forces

Figure 11 shows the normalized pull-on and pull-off forces for the elastic adhesion index α. The solid curve shown in Figure 11 represents the pull-off force predicted by Fuller and Tabor [16]. In their research, they always loaded until the applied force P equal to zero which means the contact is under zero force at the moment. Taking Figure 8 as an example (i.e. $\alpha = \frac{\sigma}{\delta_c} = 2$), the separation between nominally flat rough surface and perfect smooth surface during a loading/unloading cycle was always greater than $\bar{h}_0$. At $h = \bar{h}_0$, $P_{loading} = 0$, are compressive. As the separation decreases during loading or increases during the unloading, the total contact forces between the contacting bodies are negative, namely, are tensile forces. They focused on studying the pull-off force, whereas the pull-on force was always equal to zero during a loading cycle. Then the separation was increased (i.e. unloading cycle) after the surfaces have been compressed to the separation $\bar{h}_0$. The contact force was determined by Eqn. (30) and different from that upon loading. This force would reach a maximum tensile value $\bar{P}_m$ first and then asymptotically tended to zero as

the separation was increased until the adhesion was finally broken between the highest asperity and the smooth flat surface. The contact force $\bar{P}_m$ was the pull-off force for the whole nominally flat rough surface which contained varieties of random asperities, whereas P_c was for a single asperity in comparison. Because of the dispersion relation of asperity heights, the ratio $\bar{P}_m/NP_c$ represented adhesive reduction by Fuller and Tabor.

In this thesis, we focus on the maximum pull-on and pull-off force which will be reached during an actual loading/unloading cycle. The total forces during loading between contacting surfaces are either compressive or tensile forces which depend on the separation between the surfaces. Initially, the total forces during loading are compressive when the contact is just happening. At this moment, the adhesive forces exerted by the asperities play the main effect. As more and more asperities making contact with the flat rigid surface gradually, the contact surfaces start to repel each other. The total force becomes zero as the separation is decreased in the presence of repulsive forces. Then the forces between the surfaces will become predominately compressive and continuously increase when the surfaces are compressed into sufficiently close contact. Therefore, the balance of the adhesive forces and the repulsive forces eventually leads us to the total forces between surfaces. The maximum tensile forces during the loading cycle is the pull-on force $P_m{}'$.

For pull-off force, it will reach the maximum value as the applied load is sufficiently large. In other words, the separation between the contact surfaces need to be compressed

into a relatively small value during loading. Then unloading occurs from this relatively small separation, hence, the pull-off force will reach the maximum critical value as the contact surfaces are brought together closely enough. That is to say, the most of asperities of the nominally flat surface are making contact with the perfectly smooth and flat surface. Taking Figure 8 as an example, for adhesion index $\alpha = \frac{1}{\Delta_c} = 2.0,$ Fuller and Tabor [16] loaded until zero pull-on force which means they only studied the separation of the loading/unloading cycle was greater than 0.97. At $h = \bar{h}_0 = 0.97,\ P_{on} = P_{off} = 0$. The separation was increased upon unloading after the surfaces have been compressed to the separation $\bar{h}_0 = 0.97$. The pull-off force $\bar{P}_m = -0.1018$ when the separation $h = \bar{h}_m = 1.47$. In our investigation, to figure out the maximum pull-off force the surfaces are brought together into sufficiently close contact. When unloading starts from $h = h_0 = 0$ as we note in the figure, the pull-off force $P_m = -0.1439$ when the separation $h = h_m = 0.9$ which is different from the result of Fuller and Tabor. It is clear from the above that the tensile pull-off force is greater than the one Fuller and Tabor [16] got before. This is the reason why the maximum pull-off force we obtained is different from the pull-off force which Fuller and Tabor [16] predicted as shown in Figure 11.

From Eqn. (27), we will notice that the maximum pull-on force is a function of the elastic adhesion index α. For $\alpha = \frac{1}{\Delta_c} = 0$, the surface is theoretically smooth which means all the asperities have the same height. All the asperities of the surface make contact with

the flat smooth surface at the same time. Following the previous derivation procedure in this thesis, the normalized pull-on force for single asperity $P/P_c \approx 0.889$ in term of Eqn. (18) for $\delta/\delta_c = 0$, where P_c is the maximum force (tensile) for breaking the adhesion between the single asperity and the flat smooth surface as talked above. Meanwhile, the curve-fit results that we use throughout the thesis, $P/P_c = 0.883$ for $\delta/\delta_c = 0.01$. Therefore, the relative normalized pull-on force for amount of asperities $P_m'/NP_c = NP/NP_c = 0.883$ for $\delta/\delta_c = 0.01$ as shown in the Figure 11. Accordingly, the curve-fit function we used is proved to be effective when comparing the its result with the theoretical result 0.889 with the error is approximately equal to 0.67%. Similarly, the adhesion between all the asperities and the flat rigid surface are broken at the same time for $\alpha = \frac{1}{\Delta_c} = 0$. Hence, the relative normalized pull-off force for amount of asperities $P_m/NP_c = 1$ also shown in the Figure 11. From Figures 4-9, we will notice that the normalized separation at where maximum pull-off occurs, is larger than $\Delta_c + (h_0)_{min}$, therefore the lower limit –L of the integration in Eqn. (30) is $-\Delta_c$ which is independent of the minimum separation h_0, namely, independent of the corresponding pull-on force. The evidence suggests, therefore, the maximum pull-off force is also a function of the elastic adhesion index. However, the actual pull-on and pull-off will be reached during a loading/unloading cycle are determined by surface roughness and the extent of loading, thus, they are functions of the parameter $\alpha = \frac{1}{\Delta_c}$ and the minimum separation h_0.

For rough surfaces with large values of α, the majority of asperity heights are not likely contained within the tensile portion BD shown in Figure 3 due to the asperity heights are highly dispersed. From Figure 2, we will notice that the adhesive forces sustained by multiple low asperities will be counteracted by the compressive forces exerted by the higher asperities at any separation. Compared with a smooth surface which means standard deviation $\sigma = 0$, the effect of adhesion can be regarded as negligible fraction (i.e. less than 10% of that for smooth surfaces) for rough surfaces whose elastic adhesion index are approximately larger than 2.25. Finally, Figure 12 shows separation locations where maximum pull-on and pull-off force occurs as a function of the elastic adhesion index α.

4. CONCLUSION

We have determined the contact behavior of a multi-asperity JKR model. Rough surfaces are regarded to have variations in individual asperity heights which have a Gaussian distribution with standard deviation σ. Strong adhesion occurs between the asperities of the rough surface and the smooth surface. JKR theory has been used to formulate a load-displacement relation for the single asperity to study the influence of surface roughness on the assessment of adhesion reduction. The results are determined by a four-term curve-fit function based on the JKR theory. It is also shown that surface topography is the key factor to affect the hysteresis losses which is due to the different behaviors during a loading and unloading cycle. Hysteresis losses is a function of the parameter α and the maximum applied load. The analysis has shown that the parameter α, which is the ratio of surface roughness to adhesion extension, determines the adhesion. Compared to a smooth surface ($\alpha = 0$), the larger the roughness of surface, the smaller is the pull-off force and the hysteretic energy.

For a constant surface roughness, the loading cycle determines the pull-on force and the minimum separation between the mean level of asperity heights and the nominally smooth surface. The pull-off force during the unloading cycle depends on the maximum extent of loading as well as on the parameterα. The different loading and unloading behaviors due to adhesive forces results in hysteresis energy losses. Eventually, with

increasing applied load, the loss due to hysteresis energy is increased from zero to a maximum critical value determined by the parameter α.

When the applied load is sufficiently large, the maximum pull-on and pull-off forces are functions only of the parameter α, and are independent of maximum applied load. However, when the applied load is relatively small, the pull-on and pull-off forces are determined by the parameter α as well as the extent of loading. The theory predicts that the pull-on and pull-off forces fall to less than 10% of that for a smooth surface as the key parameter becomes greater than 1.26 and 2.25 respectively. This thesis predicts the adhesion is decreased to a negligible fraction of that for a smooth surface when the parameter α reaches 2.5. Meanwhile, the hysteresis losses decrease significantly with increasing values of parameter α.

We revise the Tabor and Fuller model [16] and predict an analytical theory for the contact of two nominally flat surfaces. However, Tabor and Fuller only focused on the effect of surface roughness on the pull-off force as they loaded the contact bodies to zero compressive force. In this thesis, the pull-on/off forces (maximum pull-on/pull-off forces, in particular) and hysteresis energy losses are obtained to study the contact adhesion. It is found that the strength of adhesion for two nominally flat surfaces is not only a function of the surface roughness of the contacting bodies, but also is determined by the extent of loading.

REFERENCES

[1] Tabor, D. and Winkerton, R.H.S. (1969). The direct measurements of normal and retarded Van der Waals forces, *Proceedings of the Royal Society of London,* **A312,** pp. 435-450.

[2] Israeachvili, J.N. and Tabor, D. (1972). The measurement of Van der Waals dispersion forces in the range 1.5 to 130 nm, *Proceedings of the Royal Society of London,* **A331,** pp. 19-38.

[3] Zhao, Y. P., Wang, L.S., and Yu, T.X. (2003). Mechanics of adhesion in MEMS- a review, *Journal of adhesion science and technology,* **17,** pp. 519-523.

[4] Maboudian, R. (1998). Surface processes in MEMS technology, *Surface Science Reports,* **30 (6),** pp. 207-269.

[5] Feyman, R.P. (1992, March). There's plenty of room at the bottom, *Journal of Microelectromechanical Systems,* **1,** pp. 60–66.

[6] Hertz.H. (1882). Über die berührung fester elastischer Körper (On the contact of rigid elastic solids). *J. reine und angewandte Mathematik,* **92,** pp. 156 -171.

[7] Yu, N. and Polycarpou. A.A. (2004). Adhesive contact based on the Lennard–Jones potential: a correction to the value of the equilibrium distance as used in the potential, *Journal of Colloid and Interface Science,* **278,** pp. 428-435.

[8] Bradley, RS. (1932). The cohesive force between solid surfaces and the surface energy of solids, *Philosophical Magazine,* **13,** pp. 853-862.

[9] Johnson, K. L., Kendall K. and Roberts, A. D. (1971). Surface energy and the contact of elastic solids, *Proceedings of the Royal Society of London,* **A324,** pp.301-313.

[10] Derjaguin, B.V., Muller, V.M. and Toporov, Y.P. (1975). Effect of contact deformations on the adhesion of particles, *Journal of Colloid and Interface Science,* **53,** pp. 314-326.

[11] Muller, V.M. and Derjaguin, B.V. and Toporov, Y.P. (1983). On two methods of calculation of the force of sticking of an elastic sphere to a rigid plane, *Colloids and Surfaces,* **7,** pp. 251-259.

[12] Tabor, D. (1977, January). Surface forces and surface interactions, *Journal of Colloid and Interface Science,* **58,** pp. 2-13.

[13] Maugis, D. (1992). Adhesion of spheres: The JKR-DMT transition using a Dugdale model, *Journal of Colloid Interface Science,* **150,** pp. 243-269.

[14] Dugdale, D.S. (1960, May). Yielding of steel sheets containing slits, *Journal of the Mechanics and Physics of Solids,* **8,** pp. 100-104.

[15] Greenwood, J.A. and Williamson, J.B.P. (1966). Contact of nominally flat surfaces, *Proceedings of the Royal Society of London,* **A295,** pp. 300-319.

[16] Tabor, D. and Fuller, N.G.D. (1975, September). The effect of surface roughness on the adhesion of elastic solids, *Proceedings of the Royal Society of London,* A345, pp. 327-342.

[17] Johnson, K.L. and Greenwood, J.A. (1997). An adhesion map for the contact of elastic spheres, *Journal of Colloid and Interface Science,* **192,** pp. 326-333.

[18] Stark, M., Moller, C., Muller, D.J. and Guckenberger, R. (2001, June). From images to interactions: high-resolution phase imaging in tapping-mode atomic force microscopy, *Biophys,* **80,** pp. 3009-18.

[19] Noy, A., Sanders, C.H., Vezenov, D.V., Wong, S.S. and Lieber, C.M. (1998, March). Chemically-sensitive imaging in tapping mode by chemical force microscopy: relationship between phase lag and adhesion, *Langmuir, 14***,** pp. 1508-1511.

[20] Tamayo, J., Garcia, R. (1996). Deformation, contact time, and phase contrast in tapping mode scanning force microscopy, *Langmuir 12*, pp. 4430-4435.

[21] Rützel, S., Lee, S.I., Raman, A. (2003, August). Nonlinear dynamics of atomic–force–microscope probes driven in Lennard–Jones potentials, *Proceedings of the Royal Society of London,* **459,** pp. 1925-1948.

[22] 1st Muller, V.M., Yushchenko, V.S., Derjaguin, B.V. (1994, April). On the influence of molecular forces on the deformation of an elastic sphere and its sticking to a rigid plane, *Journal of Colloid and Interface Science,* **77,** pp. 91-101.

[23] CIavarella, M., Greenwood, J.A., Baber, J.R. (2016). Effect of Tabor parameter on hysteresis losses during adhesive contact. J. Mech. Phys. Solids, http://dx.doi.org/10.1016/j.jmps.2016.10.005.

[24] Greenwood, J.A. (1965, October). Paper 65-Lub-10, ASLE- ASME Lubrication Conference, San Francisco.

[25] Maugis, D. (2000). Contact, adhesion and rupture of elastic solids, Springer- Verlag, Berlin, Heidelberg, New York.

[26] Johnson, K.L. (1976), Adhesion at the Contact of Solids, *Theoretical and Applied Mechanics* (Ed. W.T. Koiter), North Holland, Amsterdam

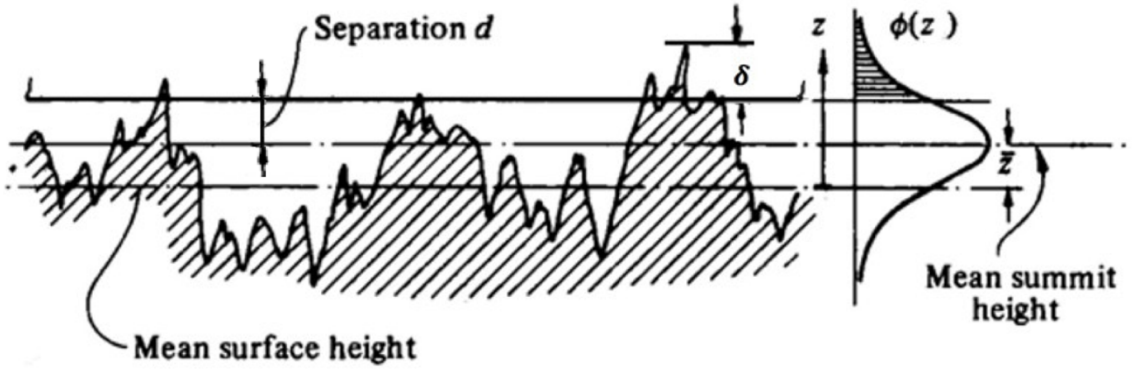

Figure 1 The contact of nominally rough surface with a rigid smooth surface. The asperity heights of the rough have a Gaussian distribution with standard deviation σ.

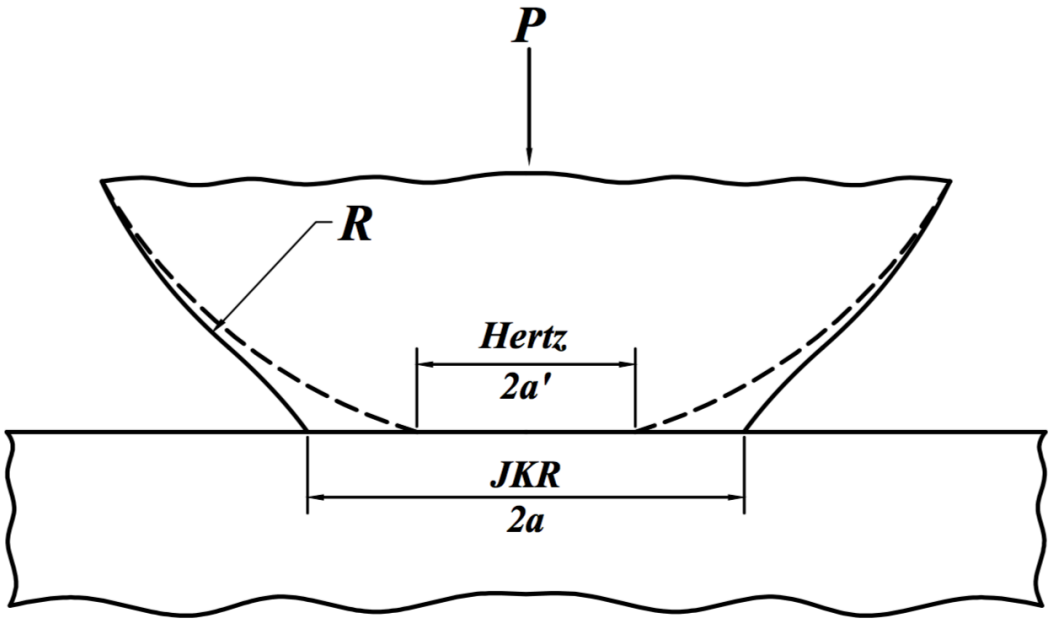

Figure 2 Schematic of contact area for the Hertz Contact and JKR model.

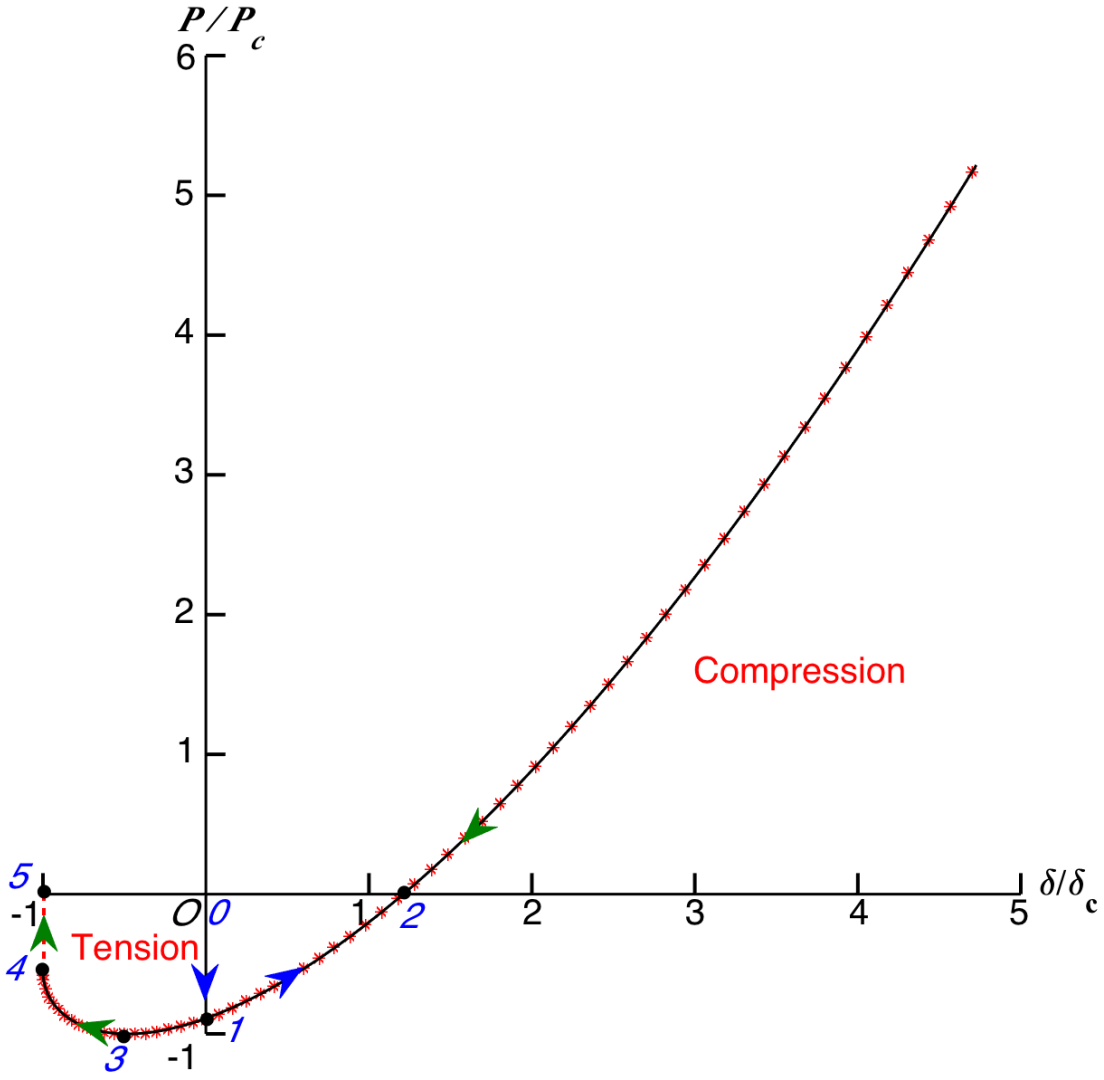

Figure 3 The relation of Load-displacement for a single asperity in the presence of adhesion. The solid line represents the original relation between P/P_c and δ/δ_c expressed by Eqns. (13) and (14), whereas the asterisks(i.e.*) represent the Four-term Curve-fit Function described by Eqn. (15).

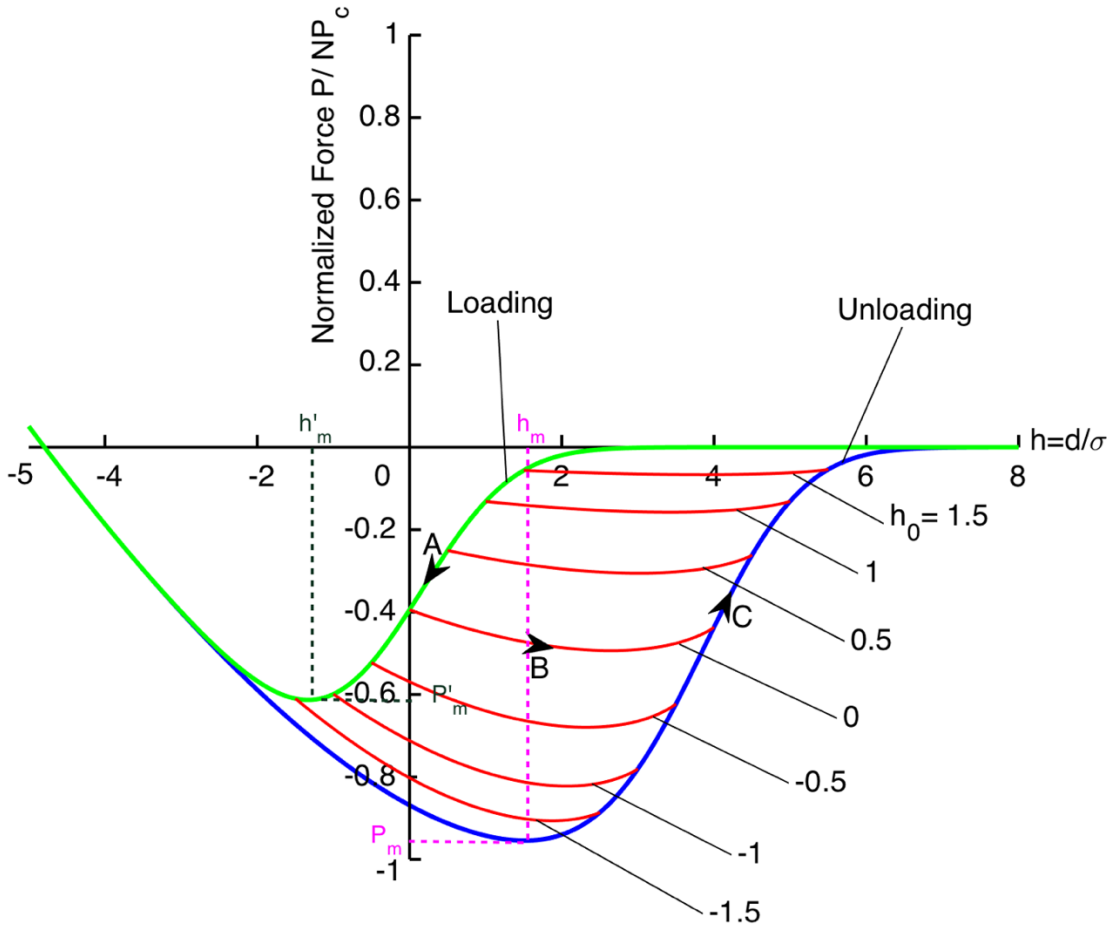

Figure 4 Normalized force P/NP_c vs. normalized separation upon loading/ unloading at $\alpha = 1/\Delta_c = 0.25$ at different values of minimum separation h_0(-1.5, -1, -0.5, 0, 0.5, 1 and 1.5). P_m represents the maximum pull-off force, whereas h_m represents the corresponding separation where P_m occurs. P'_m represents the maximum pull-on force, whereas h'_m represents the corresponding separation where P'_m occurs.

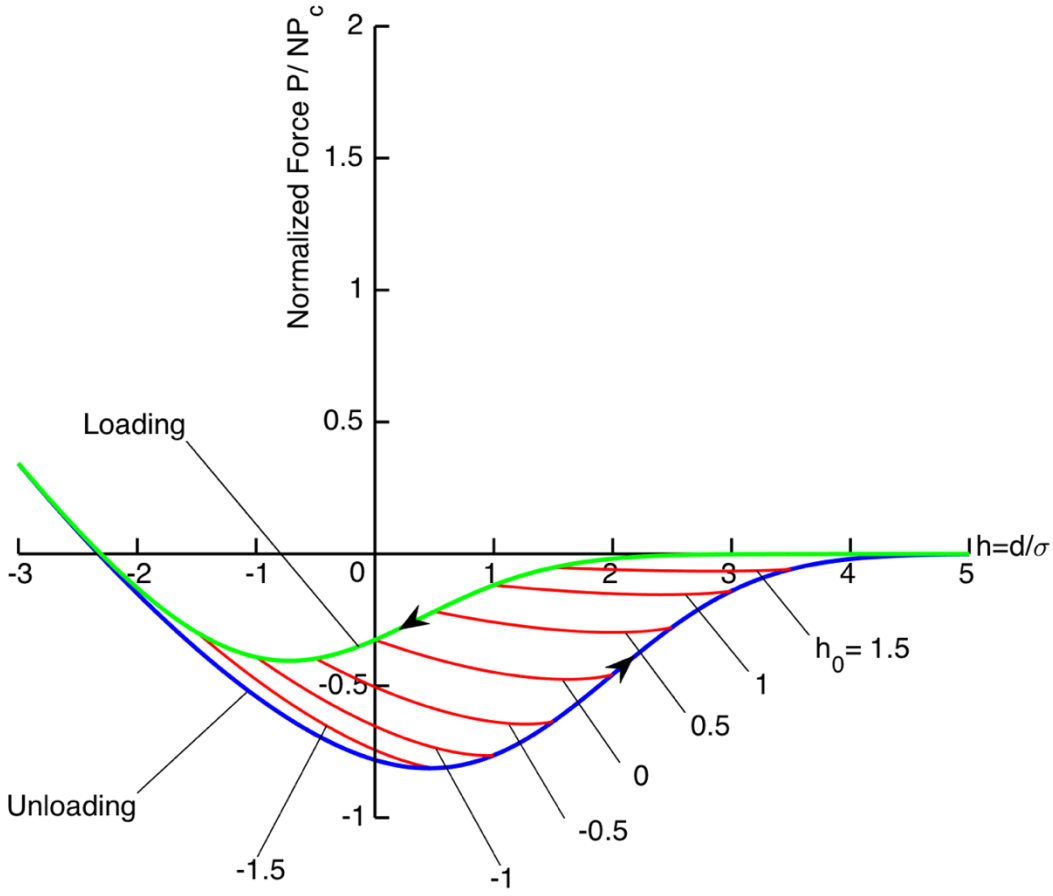

Figure 5 Normalized force P/NP_c vs. normalized separation upon loading/ unloading at $\alpha = {}^{1}/_{\Delta_c} = 0.5$ at different values of minimum separation h_0(-1.5, -1, -0.5, 0, 0.5, 1 and 1.5).

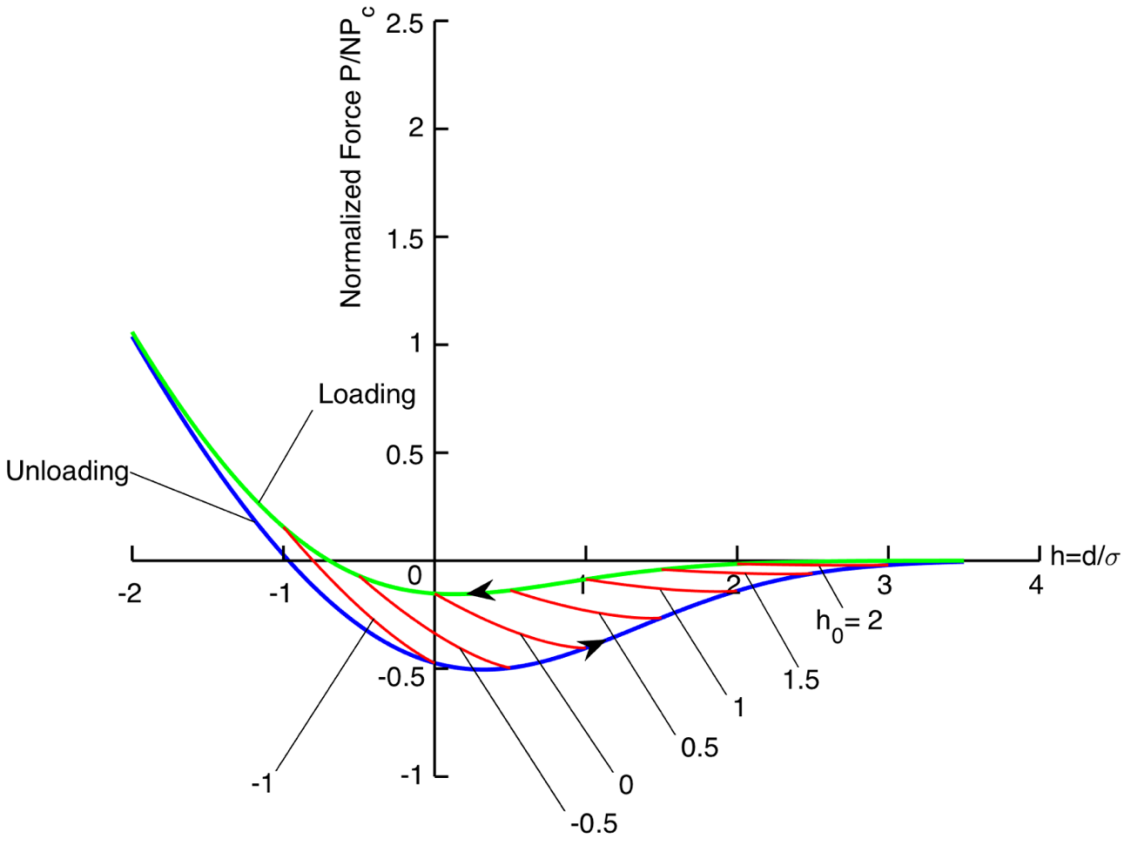

Figure 6 Normalized force P/NP_c vs. normalized separation upon loading/ unloading at $\alpha = {}^{1}/_{\Delta_c} = 1.0$ at different values of minimum separation h_0(-1, -0.5, 0, 0.5, 1, 1.5 and 2).

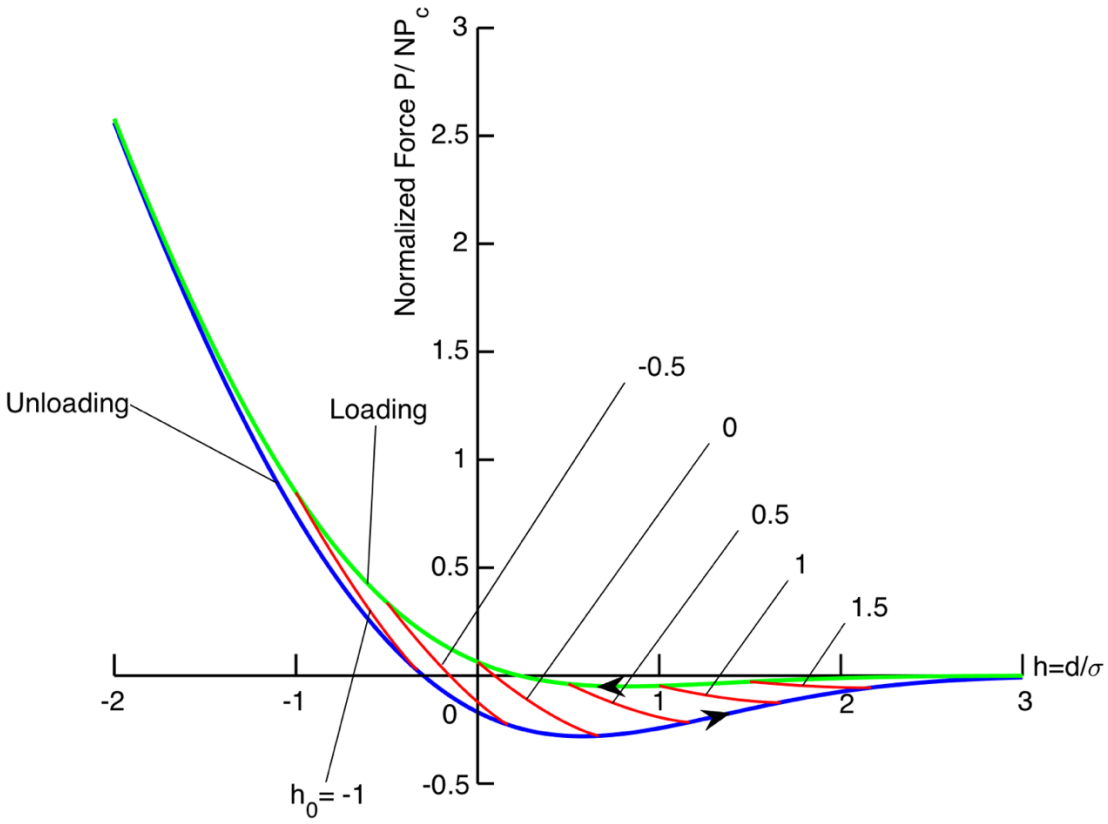

Figure 7 Normalized force P/NP_c vs. normalized separation upon loading/ unloading at $\alpha = {}^{1}/_{\Delta_c} = 1.5$ at different values of minimum separation h_0 (-1, -0.5, 0, 0.5, 1 and 1.5).

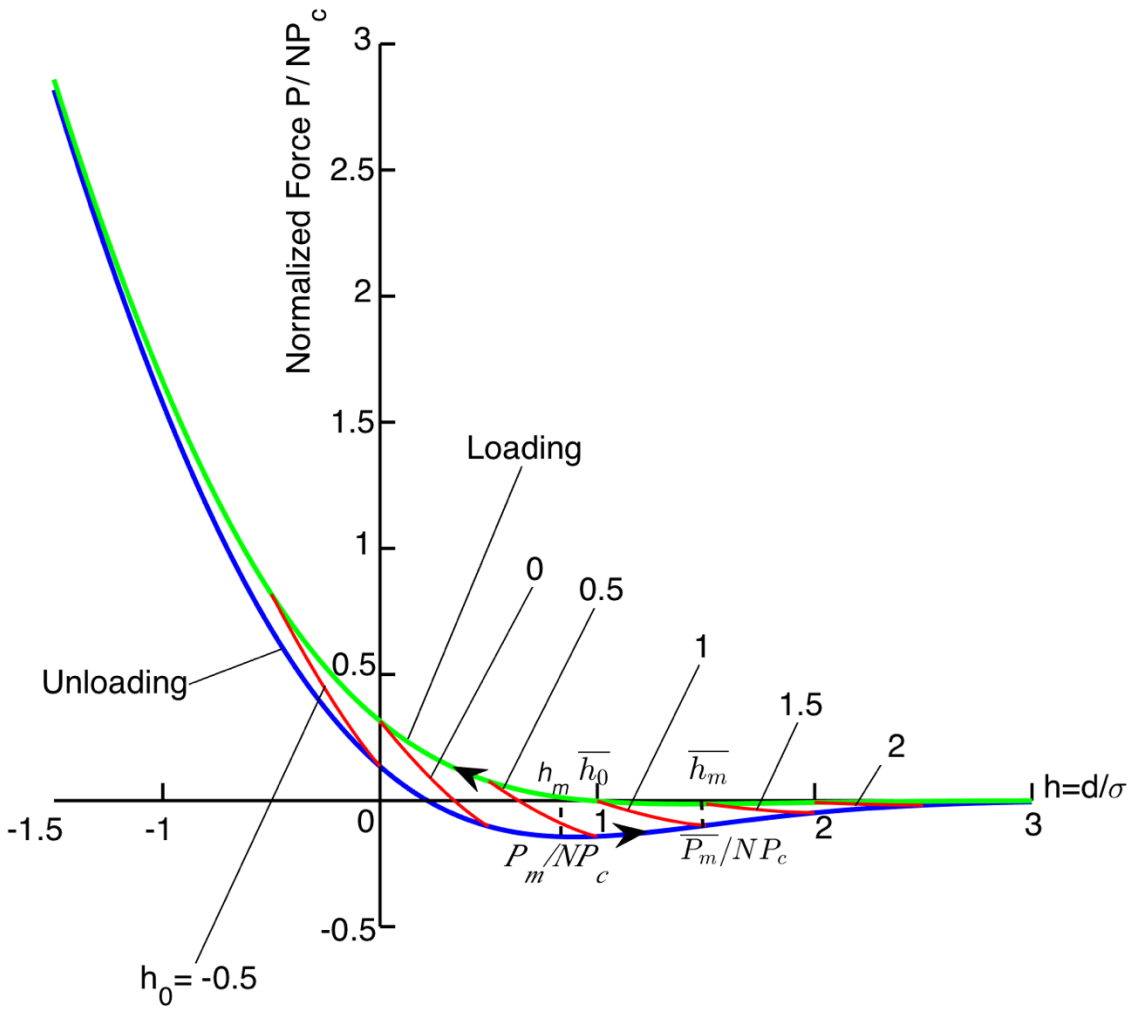

Figure 8 Normalized force P/NP_c vs. normalized separation upon loading/ unloading at $\alpha = {}^{1}/_{\Delta_c} = 2.0$ at different values of minimum separation h_0 (-0.5, 0, 0.5, 1, 1.5 and 2).

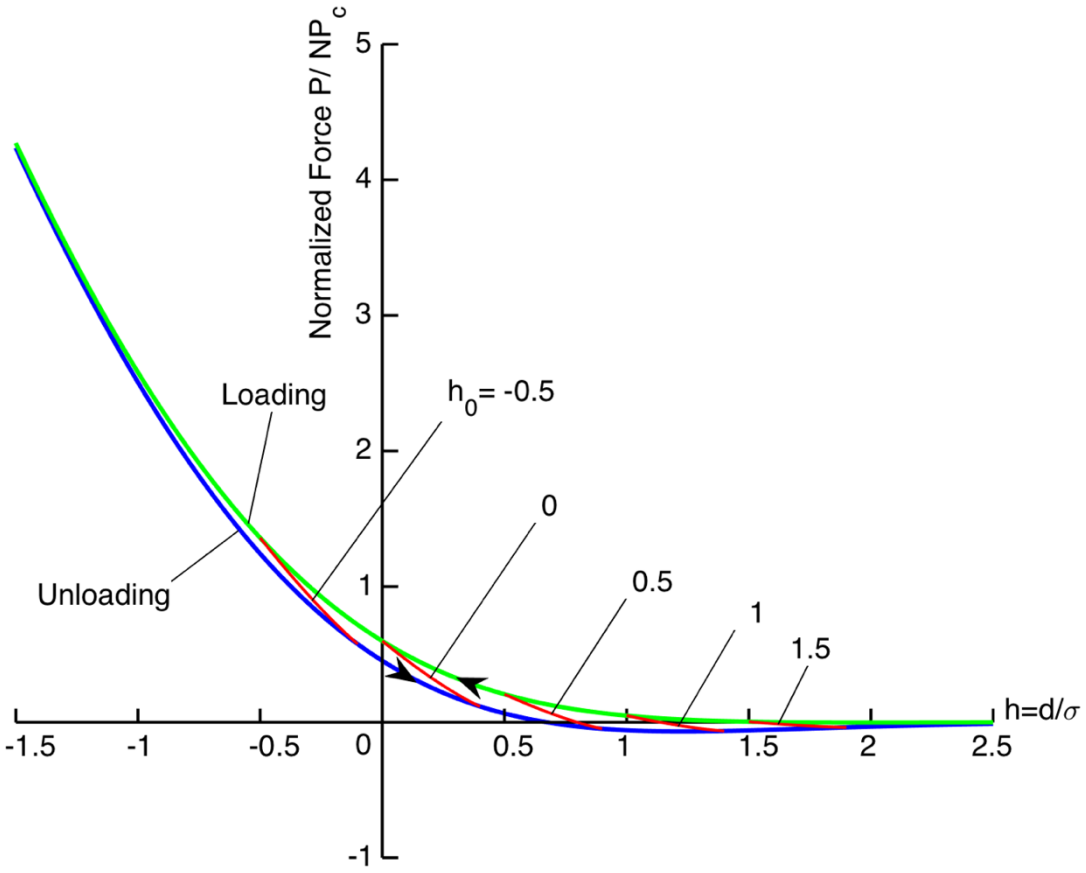

Figure 9 Normalized force P/NP_c vs. normalized separation upon loading/ unloading at $\alpha = {}^{1}/_{\Delta_c} = 2.5$ at different values of minimum separation h_0(-0.5, 0, 0.5, 1 and 1.5).

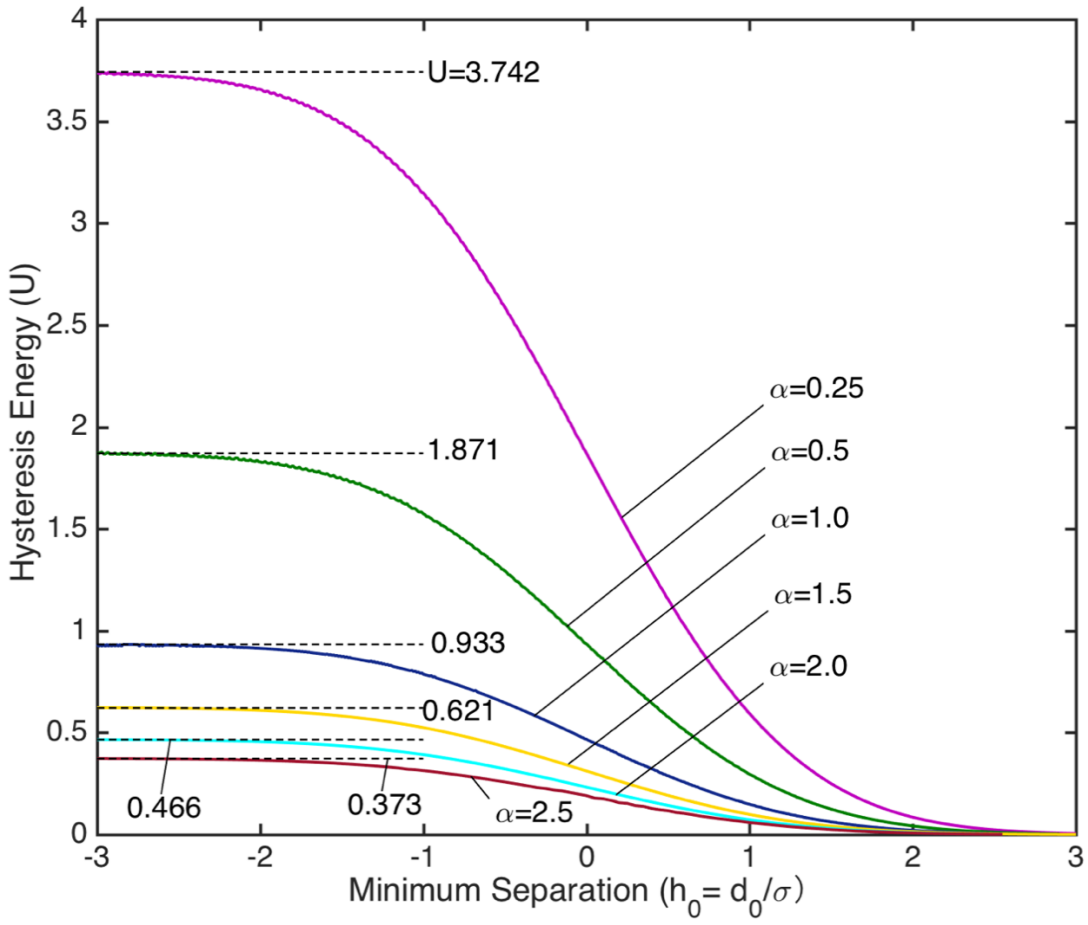

Figure 10 Hysteretic energy vs. minimum separation h_0 at different values of parameter $\alpha = {}^{1}/_{\Delta_c}$. The dashed lines represent the corresponding maximum hysteresis losses during loading and its subsequent unloading.

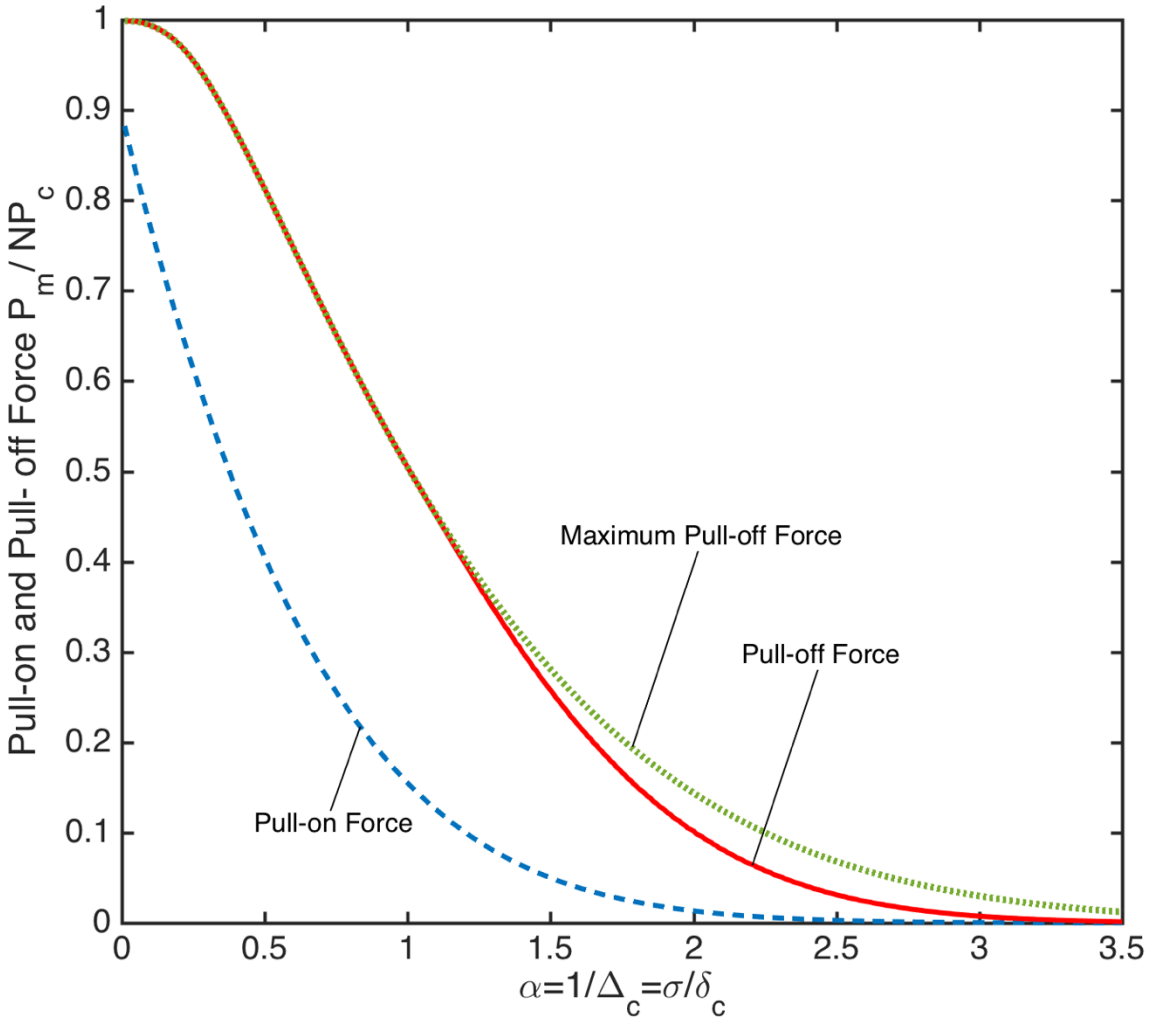

Figure 11 Dimensionless pull-on and pull-off force vs. parameter $\alpha = 1/\Delta_c$ for the contact of a deformable rough surface with a perfect smooth plane. The solid curve represents the pull-off force when unloading starts at zero total force after loading. The dot curve represents maximum pull-off force (i.e. P_m as shown in Figure. 4) when the nominally rough surface is compressed into the flat rigid surface by an enough large approach δ upon loading. The

dashed curve represents the pull-on force (i.e. P_m' as shown in Figure. 4) upon loading.

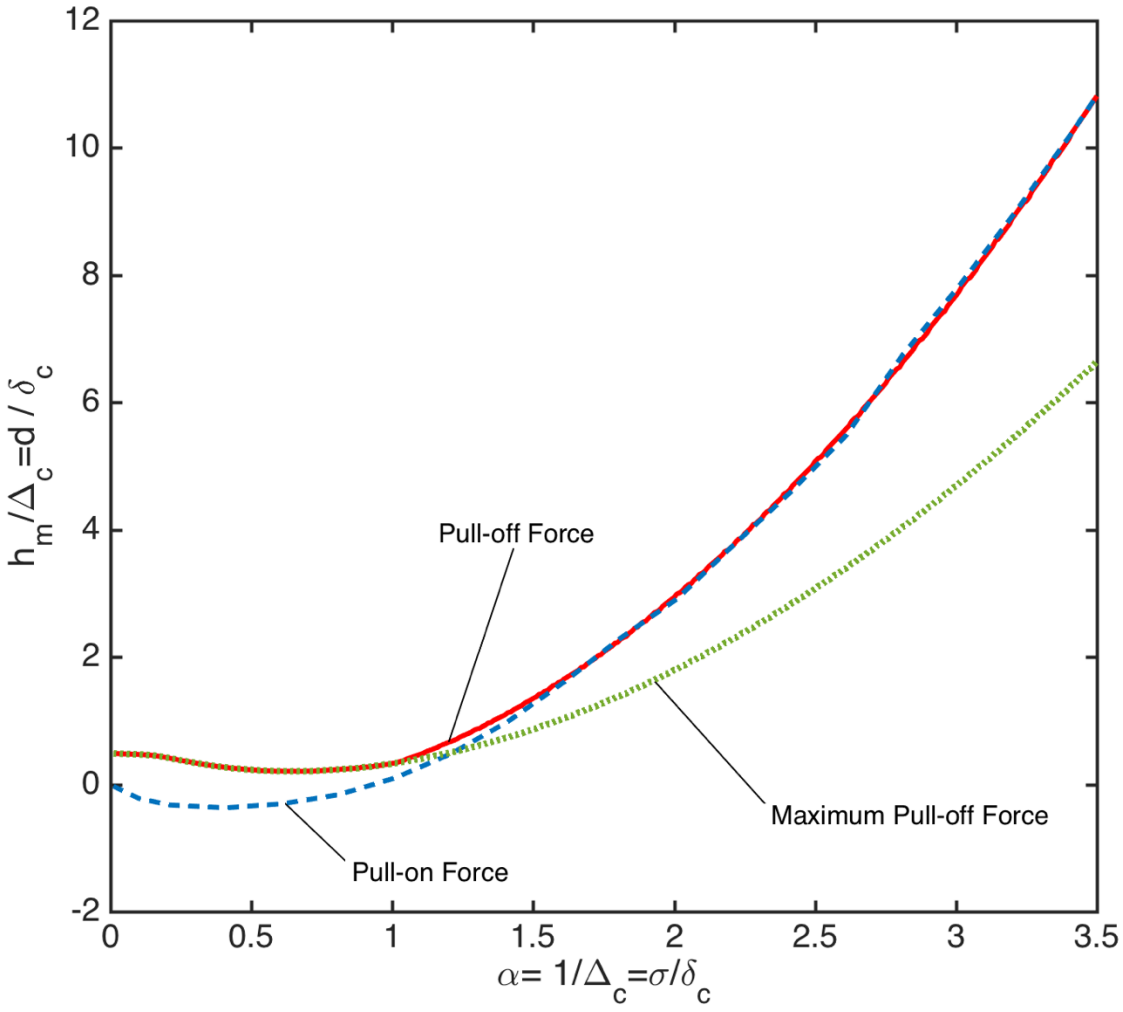

Figure 12 Separations h_m/Δ_c of pull-on and pull-off forces vs. parameter $\alpha = 1/\Delta_c$ for the contact of a deformable rough surface with a perfect smooth plane. The solid curve represents the corresponding separations of pull-off forces for different values of α, whereas the dot curve represents the separations of maximum pull-off force. The dashed curve represents the separations of maximum pull-on force.